



Field-free long-lived alignment of molecules with a two-dimensional optical centrifuge

A. A. Milner, A. Korobenko, and V. Milner

Department of Physics & Astronomy, The University of British Columbia, Vancouver, Canada

(Received 29 March 2016; published 11 May 2016)

We introduce an optical tool—a “two-dimensional optical centrifuge”—capable of aligning molecules in extreme rotational states. The alignment is studied in oxygen under ambient conditions, and in a cold jet of nitrogen. Unlike the conventional centrifuge, which confines the molecules in the plane of their rotation, its two-dimensional version aligns the molecules along a well-defined axis, similar to the effect of a single linearly polarized laser pulse, but at a much higher level of rotational excitation. We observe long lifetimes of the created alignment due to the increased robustness of ultrahigh rotational states with respect to collisions. The adiabatic nature of the centrifuge excitation provides a means of generating stationary aligned states.

DOI: [10.1103/PhysRevA.93.053408](https://doi.org/10.1103/PhysRevA.93.053408)

I. INTRODUCTION

The ability to align molecules is one of the key requirements in a growing number of areas of molecular science, from attosecond high-harmonic spectroscopy [1,2] and photoelectron spectroscopy [3], to controlling molecular interactions with atoms [4], molecules [5], and surfaces [6–8], to altering molecular trajectories in external fields [9,10] and generating THz radiation [11,12] (for recent reviews on the impact of molecular alignment on molecular dynamics, see Refs. [13–15]).

The two commonly used techniques are the adiabatic and nonadiabatic alignment with intense nonresonant laser pulses [16,17]. Similar to the alignment by static fields [18,19], adiabatic methods rely on the presence of a strong laser field during the aligned phase, which may not always be tolerated. Field-free molecular alignment is typically achieved by using the nonadiabatic interaction of a femtosecond pulse with the induced dipole moment of a molecule. Though extremely successful with cold molecular ensembles, this approach is of limited use at higher temperatures, when the required (and correspondingly higher) field strengths exceed the molecular ionization threshold.

The ionization limit can be avoided by breaking a single laser pulse into a train of pulses. Multiple schemes of using pulse trains to increase the degree of alignment have been proposed theoretically [20–23], and implemented experimentally with periodic sequences of two [24–26] and up to eight laser pulses [27,28]. However, it has been recently shown that the centrifugal bond stretching and the effect of dynamical localization limit the reach of the nonadiabatic rotational excitation with multiple laser pulses to relatively low excitation levels [29–33].

Much higher degrees of rotational excitation are available through the method of an optical centrifuge [34–37]. In contrast to the dynamics of impulsively kicked molecules, the rotation of the centrifuged molecules (known as molecular superrotors) is confined to a plane. Strong planar confinement has recently been studied experimentally by means of ion imaging [38] and by detecting the centrifuge-induced optical birefringence [39,40]. Typically, the direction of the transient alignment of superrotors within the rotation plane is random from pulse to pulse, preventing one from using the centrifuge as an instrument for aligning the molecules with respect to the laboratory frame.

Here we show that a simple modification to the centrifuge allows us to achieve molecular alignment, similar to the one induced by a femtosecond kick, simultaneous with extreme levels of rotational excitation characteristic of the centrifuge spinning. We create a two-dimensional (2D) projection of the corkscrew-shaped field of a conventional centrifuge [hereafter referred to as a three-dimensional (3D) centrifuge] by passing it through a linear polarizer. The field of a 2D centrifuge, shown in Fig. 1(a), consists of a series of pulses, all linearly polarized along the same direction. Both the individual pulse width and the time interval between the pulses are gradually decreasing from the head to the tail of the sequence.

As we demonstrate in this work, the effect of a 2D centrifuge is rather similar to that of its 3D prototype, suggesting that a “piecewise adiabaticity” [41] provides the mechanism for the accelerated rotation. The latter may be thought of as a series of adiabatic Raman transitions between the states with increasing rotational quantum number $\Delta J = 2$ [42], but constant projection of \mathbf{J} on the field polarization $\Delta M_J = 0$. Since the symmetry between positive and negative values of M_J is not broken (unlike the case of a 3D centrifuge, where ΔM_J is either $+2$ or -2) the directionality of the induced rotation is lost. In return, however, one gains the ability to fix the direction of the molecular alignment along the (now constant) field polarization.

Aligning the molecules in high J states has an immediate advantage over the conventional alignment with a femtosecond pulse [hereafter referred to as a one-dimensional (1D) kick]. As has been demonstrated in our recent work, the decay of both the rotational coherence [43] and the rotational energy [40] of molecular superrotors due to collisions is much slower than that of slowly rotating molecules. Here we compare the decay of molecular alignment, induced by a 1D kick and a 2D centrifuge in oxygen under ambient conditions, showing significantly longer decay times in the latter case.

In this work we employ three different detection techniques. Section II describes our use of Raman spectroscopy to characterize the frequency of molecular rotation and its directionality. In Sec. III we show and discuss the long lifetime of the centrifuge-induced alignment, found from measuring the optical birefringence of a dense gas of molecular superrotors. To quantify the degree of molecular alignment, produced by a 2D centrifuge, we utilize the technique of velocity map imaging described in Sec. IV. The paper concludes with a summary.

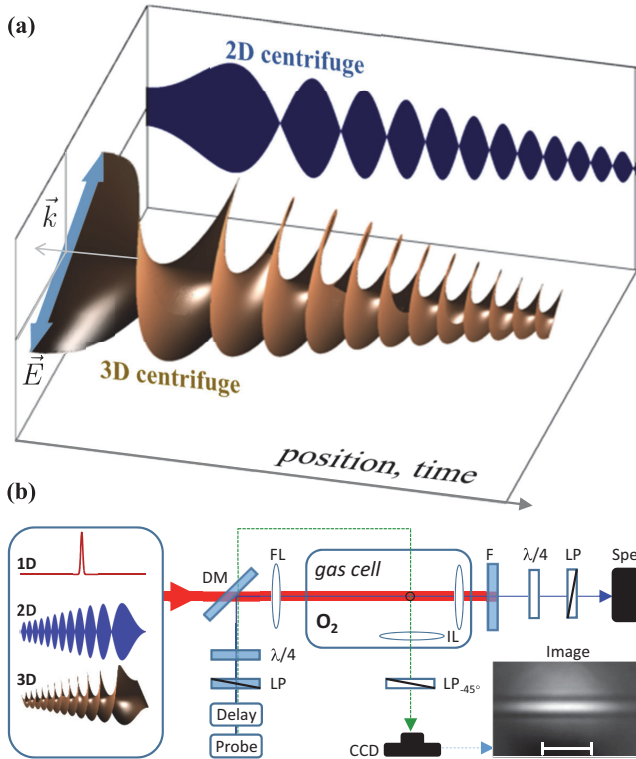


FIG. 1. (a) Illustration of the concept of a “two-dimensional (2D) centrifuge.” The three-dimensional corkscrew-shaped surface represents the field of a conventional “3D centrifuge,” propagating from right to left. Shown in blue is the field of a 2D centrifuge, created by passing the 3D centrifuge through a linear polarizer. (b) Scheme of the experimental setup for Raman spectroscopy and the detection of the centrifuge-induced optical birefringence. O_2 molecules are rotationally excited by a pump beam (thick red line) focused by a focusing lens (FL) in the middle of a gas cell (black circle). Probe pulses are delayed with respect to the pump pulses, and either directed collinearly with the pump beam by means of a dichroic mirror (DM) or sent perpendicularly to it (thin blue and dashed green lines, respectively). In the longitudinal or transverse geometry, the probe light is used to image the interaction region onto an input slit of a spectrometer (Spe) or a charge-coupled device camera (CCD), respectively, with an imaging lens (IL). Linear polarizers (LP) and quarter-wave plates are used to create different combinations of linear and circular polarizers and analyzers, as described in the text. A typical image of the cloud of centrifuged molecules is shown in the lower right corner, with a horizontal bar representing the distance of 200 μm .

II. RAMAN SPECTROSCOPY OF MOLECULAR SUPERROTORS PRODUCED BY A 2D CENTRIFUGE

The experimental configuration for analyzing the induced molecular rotation by means of coherent Raman spectroscopy (similar to our earlier work [37]) is shown in Fig. 1(b). Oxygen molecules in a gas cell are rotationally excited by either a single femtosecond pulse (1D kick), a conventional (3D) centrifuge, or its two-dimensional projection (2D centrifuge). The excitation light (thick red line) is focused inside the gas cell to a spot size of 90 μm (FWHM diameter). For a 1D kick we use a 60 fs pulse, whose total energy of 630 μJ

results in the peak intensity of 5.4×10^{13} W/cm², close to the ionization threshold of oxygen. The 3D centrifuge is produced similarly to our previous work [37] and is converted to its two-dimensional version by a linear polarizer. The duration of both the 2D and 3D centrifuge pulses is about 100 ps. Given their total energy of 10 mJ (2D) and 20 mJ (3D), the respective peak intensities are 0.75×10^{12} and 1.5×10^{12} W/cm², well below the ionization threshold. Probe pulses are 4 ps long [3.75 cm⁻¹ spectral bandwidth (FWHM) centered around 400 nm].

We send the pump and probe beams collinearly [thick red and thin blue lines in Fig. 1(b), respectively] and record the spectrum of probe pulses with a $f/4.8$ spectrometer. Owing to the induced rotational coherence, the probe spectrum develops Raman sidebands, shifted from the central probe frequency by twice the frequency of the molecular rotation. Its directionality is determined by using circularly polarized probe light as explained in detail in Ref. [37].

Raman spectrum of oxygen molecules exposed to a single intense femtosecond kick is plotted at the top of Fig. 2(a). The unshifted Rayleigh peak at 0 THz is surrounded by a series of lines indicative of the laser-induced coherent rotation, with each line corresponding to an individual $|J\rangle \rightarrow |J+2\rangle$ (Stokes) or $|J+2\rangle \rightarrow |J\rangle$ (anti-Stokes) Raman transition. The amplitude envelope of these Raman lines reflects the initial thermal rotational distribution, shifted toward higher rotational levels by $\Delta J \approx 15$, in agreement with the calculated amount of the angular momentum, transferred to the molecule by a laser pulse with intensity 5.4×10^{13} W/cm².

The result of applying a conventional (3D) optical centrifuge, with its total frequency bandwidth of about 20 THz, is shown by the blue plot at the bottom of Fig. 2(a). Aside from the low-frequency thermal envelopes, corresponding to the molecules too hot to follow the adiabatic spinning [37], the spectrum contains the response from the molecules centrifuged to the angular frequencies between 7.5 and 10 THz. Although the 3D centrifuge produces unidirectional molecular rotation (see below), linearly polarized probe scatters into both Stokes and anti-Stokes Raman sidebands (slightly asymmetric due to the residual ellipticity of the probe polarization).

Applying the 2D centrifuge results in the Raman spectra shown in the middle of Fig. 2(a). Even though the high-frequency Raman sidebands are somewhat lower than in the case of a 3D excitation (compare the lower red and blue curves), the 2D centrifuge is clearly producing molecular superrotors, spinning as fast as 9 THz. The appearance of a localized (in frequency) wave packet, well separated from the thermal envelope, indicates the adiabatic nature of the rotational excitation. Similar to its 3D prototype, the 2D centrifuge offers a high degree of control over the frequency of molecular rotation. We illustrate this by truncating the spectral bandwidth of the pulses around 8 THz, thus moving the centrifuged rotational wave packet to lower frequencies, as shown by the green plot in Fig. 2(a).

In contrast to the unidirectional rotation of a 3D centrifuge, the 2D excitation field has no preferential sense of rotation. Owing to the selection rule $\Delta M_J = 0$, the vectors of angular momentum of the molecular superrotors created by a 2D centrifuge lie in the plane perpendicular to its linear (and permanent) polarization, similar to the effect of a single 1D kick. This lack of directionality is demonstrated in

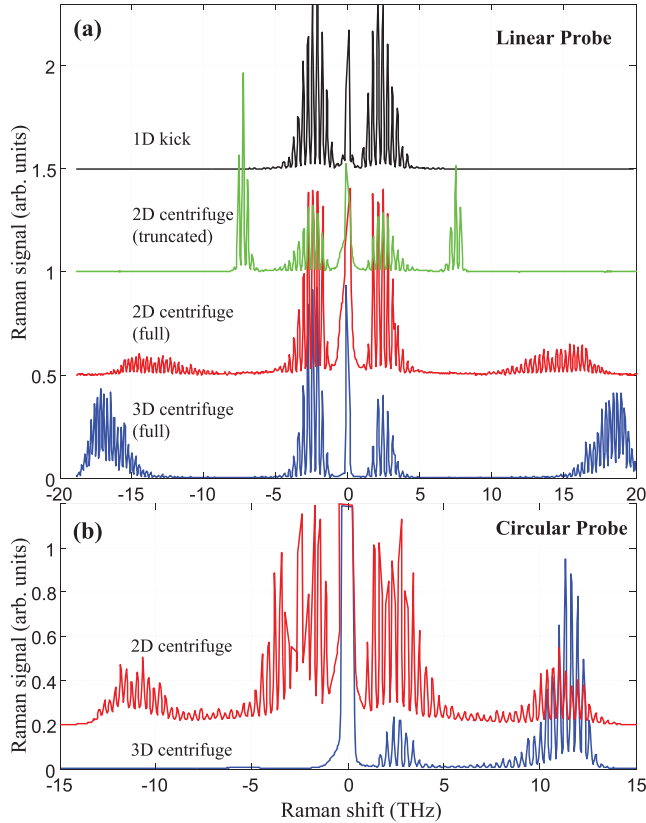


FIG. 2. (a) Rotational Raman spectra of the centrifuged oxygen molecules at room temperature and atmospheric pressure recorded with a linearly polarized probe light. From top to bottom, the spectra correspond to the excitation by a single femtosecond pulse (black), a “truncated” (see text) 2D centrifuge (green), a full 2D centrifuge (red), and a full 3D centrifuge (blue) with a terminal rotational frequency around 10 THz. The spectra have been recorded at the delay times of 400 ps. (b) Rotational Raman spectra of the centrifuged oxygen molecules recorded with a circularly polarized probe light. Upper red and lower blue curves correspond to the 2D and 3D centrifuge, respectively. The spectra have been recorded at the delay time of 400 ps.

Fig. 2(b), where we plot Raman spectra observed with a circularly polarized probe. While the missing Stokes lines in the lower (blue) spectrum indicate that the 3D-centrifuged molecules rotate in the direction opposite to the circular probe polarization [37], the presence of both Stokes and anti-Stokes Raman peaks on the upper (red) plot confirms no preferential sense of rotation induced by the 2D centrifuge.

III. OPTICAL BIREFRINGENCE OF THE GAS OF MOLECULAR SUPERROTORS PRODUCED BY A 2D CENTRIFUGE

To illustrate and compare the effects of the two centrifuge geometries, 2D and 3D, on the molecular alignment, we calculate the wave function of a rigid rotor adiabatically transferred from $|N = 1\rangle$ (the ground rotational state of O_2 which constitutes the majority of the centrifuged molecules, even if the centrifuge is applied to a room-temperature ensemble) to $|N = 19\rangle$, with each state split into three

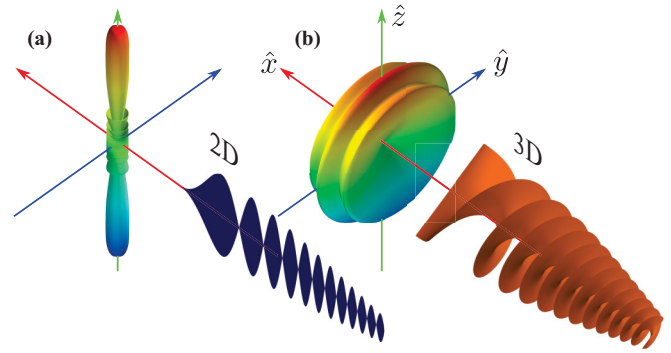


FIG. 3. Simulated molecular distribution after the rotational excitation by a 2D (a) and a 3D (b) optical centrifuge, propagating along the \hat{x} axis. See text for details.

spin-rotational components $J = N, N \pm 1$. The relatively low rotational angular momentum of the final state is chosen for illustration purposes. Although we routinely spin oxygen to $N > 100$, the calculated distributions become extremely narrow at higher values of N . After adding together the squared amplitudes of the spherical harmonics corresponding to the equally populated initial M_J states, we plot the results in Fig. 3. A 2D centrifuge is seen to produce a well-aligned ensemble, shown in Fig. 3(a), whereas the effect of a 3D centrifuge is very different: molecules are confined in the plane of their rotation, but exhibit no preferential alignment axis, as seen in Fig. 3(b).

The shape of the molecular distributions depicted in Fig. 3 can be verified by measuring the optical birefringence of the superrotors in the xz and yz planes. To probe the yz anisotropy, we again send our probe pulses collinear with the centrifuge beam (i.e., along \hat{x}), pass them between two crossed polarizers set at $\pm 45^\circ$ to \hat{z} , and record the amplitude of the Rayleigh peak in the probe spectrum as a function of the delay between the probe and centrifuge pulses. The results are shown in Fig. 4(a). No permanent birefringence is detected in the case of the 3D spinning (bottom blue circles), as one would expect for a disk-shaped distribution. On the other hand, we observe a nonzero optical birefringence induced by the 2D centrifuge, shown by red diamonds. The anisotropy axis is parallel to the linear polarization of the centrifuge pulse (\hat{z}), which was evident from the disappearance of the signal in the case of a vertically polarized probe (not shown), hence confirming the anticipated permanent molecular alignment of Fig. 3(a).

To probe the anisotropy in the xz plane, we switch to the transverse geometry with probe pulses crossing the rotationally excited molecules perpendicularly to the direction of the excitation beam [dashed green line in Fig. 1(b)]. We use this probe beam to image the cloud of molecular superrotors onto a CCD camera. The input probe polarization is set to linear at 45 deg with respect to the vertical axis. Setting an output linear polarizer at 90 deg to the input one, ensures that the recorded images reflect the centrifuge-induced birefringence in an otherwise isotropic oxygen gas. A typical image, taken 350 ps after the arrival of the centrifuge pulse, is shown in the lower right corner of Fig. 1(b). The image reveals a birefringent channel in the direction of the centrifuge beam, owing to the gyroscopic motion of the molecules [40]. The integral of the

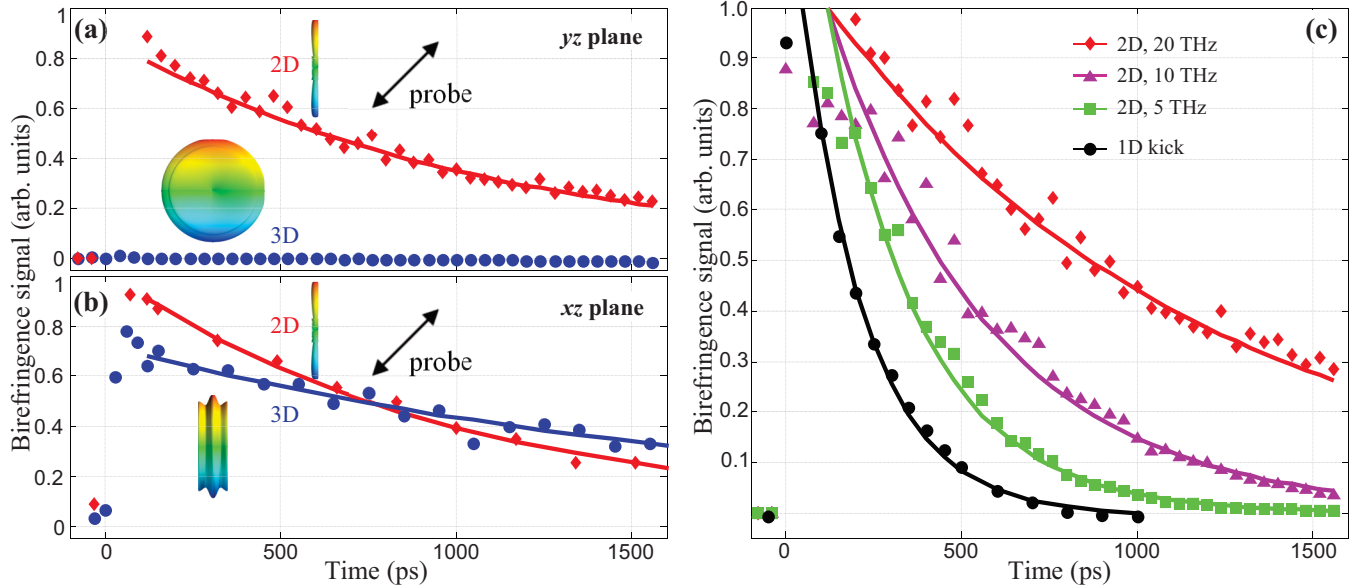


FIG. 4. Decay of the permanent birefringence of the rotationally excited oxygen gas at room temperature and atmospheric pressure in yz (a) and xz (b) planes. Red diamonds and blue circles correspond to the excitation by a 2D and a 3D centrifuge, respectively. Incident probe polarization, shown by the black arrow, is at 45 deg to \hat{z} . The calculated distributions of molecular axes are shown to illustrate the anticipated linear anisotropy for each case. (c) Comparison of the birefringence decay for the 2D centrifuge with a full spectral bandwidth of 20 THz (red diamonds) and with its bandwidth truncated at ≈ 10 THz (purple triangles) and $\lesssim 5$ THz (green squares). Black circles represent the case of a 1D kick. In all plots, solid lines show the fits by exponential decays.

transmitted probe intensity, hereafter referred to as the image contrast, is used as a measure of the gas birefringence.

Applying the 2D centrifuge results in the nonzero linear birefringence [red diamonds in Fig. 4(b)], decaying similarly to that observed in the yz plane and, therefore, confirming the rod-shaped molecular distribution. On the other hand, the disk-shaped distribution created by the 3D centrifuge, while isotropic in the yz plane, exhibits an anisotropic xz projection which gives rise to the optical birefringence, shown by blue circles in Fig. 4(b). We attribute the difference between the observed decay times (970 ± 41 and 1850 ± 138 ps for the 2D and 3D cases, respectively) to the rather different compositions of the two created rotational wave packets. The latter can be appreciated by inspecting the corresponding Raman spectra in Fig. 2(b). Although the rotational frequency of superrotors is similar in both cases, their relative weight with respect to the low-frequency rotors is much higher in the case of the 3D centrifuge (blue curve) as compared to the 2D case (red curve). Since a 3D centrifuge is always more efficient than its 2D derivative, the decay rate is always slower for a 3D than for a 2D case, although not necessarily by a factor of 2, as in the data of Fig. 4(b). Because the superrotors collide predominantly with noncentrifuged molecules, the higher the fraction of the fast spinners, the slower the decay. Determining the difference in the collisional cross sections between the disk-shaped and rod-shaped distributions, which may also contribute to the unequal birefringence decay rates, requires further investigation.

Similar to the decoherence rate of molecular superrotors [43], the decay of the permanent molecular alignment becomes slower for faster rotating molecules due to the increased adiabaticity of collisions [40,44]. We demonstrate this effect by comparing the decay rates of the birefringence

signal observed with the 2D centrifuges which have different spectral bandwidths and, therefore, different terminal rotational frequencies. As shown in Fig. 4(c), increasing the centrifuge bandwidth from $\lesssim 5$ THz (green squares) to ≈ 8 THz (purple triangles) and 20 THz (red diamonds), results in the respective increasing of the exponential decay time from 269 ± 9 to 461 ± 15 and 1094 ± 142 ps.

Also plotted in Fig. 4(c) is the decay of the permanent molecular alignment induced by a single femtosecond (1D) kick (black circles). One can clearly see the noticeably shorter lifetime of this alignment (187 ± 8 ps) with respect to that offered by a 2D centrifuge. Similar to the previously discussed increasing decay rates with a slower centrifuge, the effect stems from the lower adiabaticity of collisions between the molecules exposed to a 1D kick in comparison to those excited by a 2D centrifuge.

IV. MOLECULAR ALIGNMENT BY A 2D CENTRIFUGE

To determine the degree of molecular alignment produced by a 2D optical centrifuge, we employed the method of velocity-map imaging (VMI) [45]. The experimental configuration is shown in Fig. 5(a). A supersonic expansion through a 150- μm -diameter pulsed Even-Lavie valve cooled the nitrogen gas down to the rotational temperature of ~ 10 K, with most molecules occupying the rotational ground state. An intense linearly polarized 40 fs laser pulse Coulomb exploded the molecules into the ion fragments. For the peak intensities of $< 10^{15}$ W/cm 2 , used here, the main source of anisotropy in Coulomb explosion of N_2 stems from the geometric alignment effect [46], with the fragment ions recoiling in the direction of the internuclear axis prior to ionization. The ions were then extracted with a dc electric field along the probe polarization

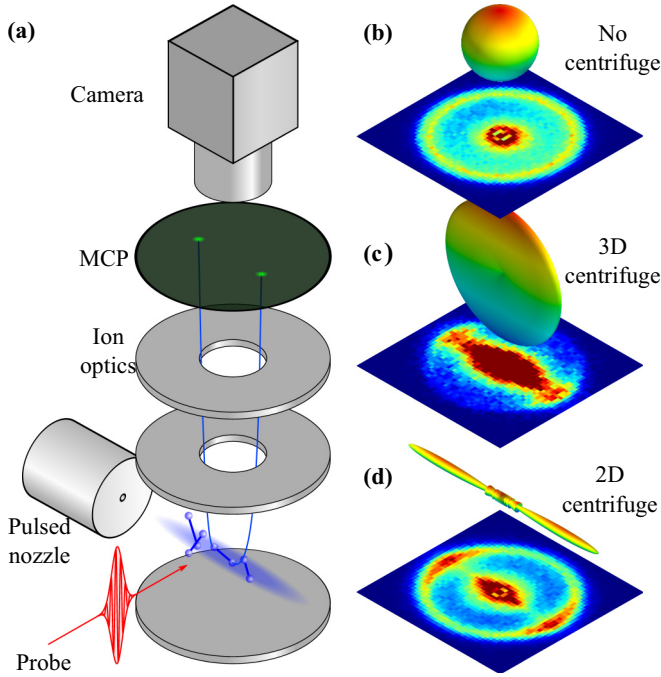


FIG. 5. (a) VMI setup, used for measuring the degree of molecular alignment of N_2 , induced by a 2D centrifuge. See text for details. Ion images of nitrogen molecules prior to any rotational excitation (b), and following the excitation by a 3D (c) and a 2D (d) centrifuge. Calculated molecular distributions are shown above the respective images.

and imaged on a phosphor screen of a microchannel plate detector (MCP). The latter was gated in time to mass-select N^+ ions, originated predominantly from the $N_2^{2+} \rightarrow N^+ + N^+$ dissociation channel. Each image was averaged over 500 000 ionization events.

In the absence of rotational excitation, the observed images were circularly symmetric, in accordance with the symmetry of the initial ensemble, as shown in Fig. 5(b). Applying either a 3D or 2D centrifuge resulted in anisotropic VMI images, plotted in Figs. 5(c) and 5(d), respectively, reflecting highly anisotropic angular distributions of the centrifuged molecules.

Since the molecular distribution $f(r, \theta, \phi)$, produced by a 2D centrifuge, is axially symmetric, its two-dimensional cross section $f(r, \theta, 0)$, containing the axis of symmetry, completely characterizes the degree of the induced alignment [see Fig. 6(a) for the definition of the relevant spherical and polar coordinates]. In this case, the alignment factor is commonly expressed as $\langle \cos^2 \theta_{2D} \rangle = \int \cos^2(\theta) f(r_0, \theta, 0) dr_0$, where $r_0 = v_0 t$ is the radial distance covered by the ion of interest, released from the Coulomb explosion with velocity v_0 , during the time of flight t .

The experimentally recorded ion images provide us with the projection $F(R, \Theta)$ of the molecular distribution $f(r, \theta, \phi)$ onto the (xz) plane. The two distributions are related to one another through the well-known Abel transform [47]

$$F(R, \Theta) = \int_R^{+\infty} \frac{r f(r, \theta, \phi)}{\sqrt{r^2 - R^2}} dr, \quad (1)$$

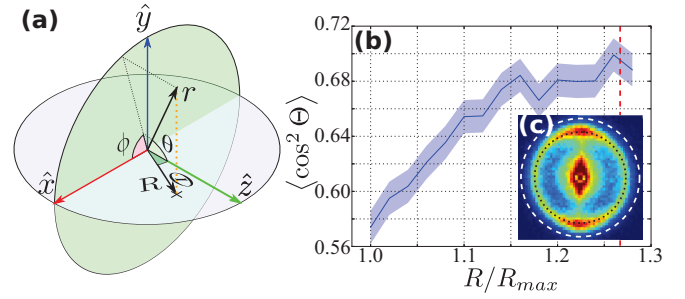


FIG. 6. (a) Definition of the spherical coordinates (r, θ, ϕ) and polar coordinates (R, Θ) used to describe the full molecular distribution and its two-dimensional projection on the (xz) plane of the ion detector. (b) R dependence of the extracted alignment factor, with the shaded region indicating the experimental error. (c) Ion image of N_2 molecules aligned with a 2D optical centrifuge. The black dotted and white dashed lines show the circular cross sections at the radius of a maximum ion signal $R = R_{\max}$, and the bigger radius used for estimating the true two-dimensional alignment factor, respectively. The latter is also marked by the red dashed line in (b).

with $\theta = \arccos \frac{R \cos \Theta}{r}$ and $\phi = \arccos \frac{\tan \Theta}{\tan \theta}$. We note that if the velocity distribution falls off quickly away from its average value v_0 and if R is sufficiently large, the integral in Eq. (1) will be accumulated mostly around its lower limit $r \approx R$. In this case, the observed angular distribution $F(R, \Theta)$ becomes proportional to $f(R, \Theta, 0)$, and the true two-dimensional alignment factor can be approximated as $\langle \cos^2 \theta_{2D} \rangle \approx \langle \cos^2 \Theta \rangle$. Following this argument, we extracted the angular distributions at various radii and calculated the corresponding values of $\langle \cos^2 \Theta \rangle$ as a function of R . As shown in Fig. 6(b), the latter indeed saturates at large R 's [white dashed circle in Fig. 6(c)], reaching the value of 0.69.

The retrieved two-dimensional alignment factor of 0.69 is still considerably lower than $\langle \cos^2 \theta_{2D} \rangle = \int Y_J^{0*}(\theta, 0) \cos^2 \theta Y_J^0(\theta, 0) d\theta = 0.87$, anticipated for the rotational quantum state $J = 85$ accessed by our centrifuge. We attribute this disagreement to the following two reasons. First, as R increases, dissociation channels other than $N_2^{2+} \rightarrow N^+ + N^+$ may provide a non-negligible contribution to the number of N^+ ions, smearing the angular distribution and lowering the extracted alignment factor.

Another important correction to our estimate of $\langle \cos^2 \theta_{2D} \rangle$ stems from the drift effect owing to the high rotational frequencies of molecular superrotors [48]. The rotational energy of the centrifuged nitrogen, studied here, reached 1.8 eV/molecule, becoming compatible with the Coulomb explosion energy release of 6.6 eV/molecule [49]. As a result, the recoil velocities of the fragment ions deviated from the internuclear axis of the exploding molecule and the measured velocity distribution no longer represented the molecular angular distribution.

V. SUMMARY

To summarize, we proposed, implemented, and studied a method of inducing molecular alignment with intense nonresonant laser pulses. The new tool of a “two-dimensional” optical centrifuge has been introduced conceptually and demonstrated

experimentally. We showed that the 2D centrifuge is capable of aligning molecules in extreme rotational states, i.e., creating aligned ensembles of molecular superrotors. Owing to the increased robustness of superrotors with respect to collisions, the method offers a way of producing long-lived alignment in dense gases. Applying the 2D centrifuge to cold or $|M_J = 0\rangle$ state-selected molecules will result in a high degree of alignment. Finally, the adiabatic spinning mechanism of the centrifuge offers two distinct advantages in comparison to the nonadiabatic rotational excitation with a single femtosecond pulse or a series of pulses. First, efficient excitation of almost any molecule with an anisotropic polarizability can be executed without changing the centrifuge

parameters. Second, the adiabatic excitation should enable transferring the molecules into a single $|J \gg 1, M_J = 0\rangle$ state, corresponding to the truly permanent (as opposed to the time-averaged) field-free molecular alignment. The latter could be instrumental in studying multiple steric effects in molecular collisions, since in most collisional processes, the exact time of collision cannot be controlled on a femtosecond time scale.

ACKNOWLEDGMENT

This research has been supported by the grants from CFI, BCKDF, and NSERC.

-
- [1] K. T. Kim, D. M. Villeneuve, and P. B. Corkum, *Nat. Photon.* **8**, 187 (2014).
- [2] F. Lepine, M. Y. Ivanov, and M. J. J. Vrakking, *Nat. Photon.* **8**, 195 (2014).
- [3] A. Stolow and J. G. Underwood, in *Advances in Chemical Physics*, edited by S. A. Rice (John Wiley and Sons, New York, 2008), Vol. 139, p. 497.
- [4] K. Tilford, M. Hoster, P. M. Florian, and R. C. Forrey, *Phys. Rev. A* **69**, 052705 (2004).
- [5] L. Vattuone, L. Savio, F. Pirani, D. Cappelletti, M. Okada, and M. Rocca, *Prog. Surf. Sci.* **85**, 92 (2010).
- [6] E. W. Kuipers, M. G. Tenner, A. W. Kleyn, and S. Stolte, *Nature (London)* **334**, 420 (1988).
- [7] R. N. Zare, *Science* **279**, 1875 (1998).
- [8] Y. Khodorkovsky, J. R. Manson, and I. Sh. Averbukh, *Phys. Rev. A* **84**, 053420 (2011).
- [9] S. M. Purcell and P. F. Barker, *Phys. Rev. Lett.* **103**, 153001 (2009).
- [10] E. Gershnabel and I. Sh. Averbukh, *Phys. Rev. Lett.* **104**, 153001 (2010).
- [11] A. G. York and H. M. Milchberg, *Opt. Express* **16**, 10557 (2008).
- [12] S. Fleischer, Y. Zhou, R. W. Field, and K. A. Nelson, *Phys. Rev. Lett.* **107**, 163603 (2011).
- [13] Y. Ohshima and H. Hasegawa, *Int. Rev. Phys. Chem.* **29**, 619 (2010).
- [14] S. Fleischer, Y. Khodorkovsky, E. Gershnabel, Y. Prior, and I. Sh. Averbukh, *Isr. J. Chem.* **52**, 414 (2012).
- [15] M. Lemesko, R. V. Krems, J. M. Doyle, and S. Kais, *Mol. Phys.* **111**, 1648 (2013).
- [16] H. Stapelfeldt and T. Seideman, *Rev. Mod. Phys.* **75**, 543 (2003).
- [17] T. Seideman and E. Hamilton, in *Advances In Atomic, Molecular, and Optical Physics*, edited by P. R. Berman and C. C. Lin (Academic Press, New York, 2005), Vol. 52, p. 289.
- [18] B. Friedrich and D. R. Herschbach, *Nature (London)* **353**, 412 (1991).
- [19] B. Friedrich and D. R. Herschbach, *Z. Phys. D* **24**, 25 (1992).
- [20] I. Sh. Averbukh and R. Arvieu, *Phys. Rev. Lett.* **87**, 163601 (2001).
- [21] M. Leibscher, I. Sh. Averbukh, and H. Rabitz, *Phys. Rev. Lett.* **90**, 213001 (2003).
- [22] M. Leibscher, I. Sh. Averbukh, and H. Rabitz, *Phys. Rev. A* **69**, 013402 (2004).
- [23] D. Sugny, A. Keller, O. Atabek, D. Daems, C. M. Dion, S. Guérin, and H. R. Jauslin, *Phys. Rev. A* **72**, 032704 (2005).
- [24] K. F. Lee, I. V. Litvinyuk, P. W. Dooley, M. Spanner, D. M. Villeneuve, and P. B. Corkum, *J. Phys. B* **37**, L43 (2004).
- [25] C. Z. Bisgaard, M. D. Poulsen, E. Peronne, S. S. Viftrup, and H. Stapelfeldt, *Phys. Rev. Lett.* **92**, 173004 (2004).
- [26] D. Pinkham and R. R. Jones, *Phys. Rev. A* **72**, 023418 (2005).
- [27] J. P. Cryan, P. H. Bucksbaum, and R. N. Coffee, *Phys. Rev. A* **80**, 063412 (2009).
- [28] S. Zhdanovich, C. Bloomquist, J. Floß, I. Sh. Averbukh, J. W. Hepburn, and V. Milner, *Phys. Rev. Lett.* **109**, 043003 (2012).
- [29] J. Floß, S. Fishman, and I. Sh. Averbukh, *Phys. Rev. A* **88**, 023426 (2013).
- [30] J. Floß and I. Sh. Averbukh, *Phys. Rev. Lett.* **113**, 043002 (2014).
- [31] J. Floß, A. Kamalov, I. Sh. Averbukh, and P. H. Bucksbaum, *Phys. Rev. Lett.* **115**, 203002 (2015).
- [32] A. Kamalov, D. W. Broege, and P. H. Bucksbaum, *Phys. Rev. A* **92**, 013409 (2015).
- [33] M. Bitter and V. Milner, [arXiv:1603.06918](https://arxiv.org/abs/1603.06918).
- [34] J. Karczmarek, J. Wright, P. Corkum, and M. Ivanov, *Phys. Rev. Lett.* **82**, 3420 (1999).
- [35] D. M. Villeneuve, S. A. Aseyev, P. Dietrich, M. Spanner, M. Y. Ivanov, and P. B. Corkum, *Phys. Rev. Lett.* **85**, 542 (2000).
- [36] L. Yuan, S. W. Teitelbaum, A. Robinson, and A. S. Mullin, *Proc. Natl. Acad. Sci. USA* **108**, 6872 (2011).
- [37] A. Korobenko, A. A. Milner, and V. Milner, *Phys. Rev. Lett.* **112**, 113004 (2014).
- [38] A. Korobenko and V. Milner, *J. Phys. B* **48**, 164004 (2015).
- [39] A. A. Milner, A. Korobenko, J. Floß, I. Sh. Averbukh, and V. Milner, *Phys. Rev. Lett.* **115**, 033005 (2015).
- [40] A. A. Milner, A. Korobenko, K. Rezaiezhadeh, and V. Milner, *Phys. Rev. X* **5**, 031041 (2015).
- [41] S. Zhdanovich, E. A. Shapiro, M. Shapiro, J. W. Hepburn, and V. Milner, *Phys. Rev. Lett.* **100**, 103004 (2008).
- [42] N. V. Vitanov and B. Girard, *Phys. Rev. A* **69**, 033409 (2004).
- [43] A. A. Milner, A. Korobenko, J. W. Hepburn, and V. Milner, *Phys. Rev. Lett.* **113**, 043005 (2014).

- [44] Y. Khodorkovsky, U. Steinitz, J.-M. Hartmann, and I. Sh. Averbukh, *Nat. Commun.* **6**, 7791 (2015).
- [45] A. T. J. B. Eppink and D. H. Parker, *Rev. Sci. Instrum.* **68**, 3477 (1997).
- [46] M. Kenzo, S. Takayuki, and N. Didier, *J. Phys. B* **37**, 753 (2004).
- [47] J. G. Underwood, I. Procino, L. Christiansen, J. Maurer, and H. Stapelfeldt, *Rev. Sci. Instrum.* **86**, 073101 (2015).
- [48] A. Korobenko, J. W. Hepburn, and V. Milner, *Phys. Chem. Chem. Phys.* **17**, 951 (2015).
- [49] A. Hishikawa, A. Iwamae, K. Hoshina, M. Kono, and K. Yamanouchi, *Chem. Phys. Lett.* **282**, 283 (1998).